Electronic Supplementary Material (ESI) for ChemComm.

Supporting Information

Multi-Responsive Luminescent Coordination Polymer Nanosheets for Selective Detection of Nitroaromatics

Ting Pan, Peng Wu, Weina Zhang, Yu Shen* and Fengwei Huo*

Key Laboratory of Flexible Electronics (KLOFE), Institute of Advanced Materials (IAM), Nanjing Tech University, 30 South Puzhu Road, Nanjing 211816, China

E-mail: iamfwhuo@njtech.edu.cn, iamyshen@njtech.edu.cn

General Information

Tricarboxytriphenylamine (TCA) was synthesized according to the reported reference.[1] All chemicals and solvents were purchased from commercial sources and used without further purification. Lanthanum nitrate hydrate ($La(NO_3)_3 \cdot xH_2O$) was purchased from Alfa. N,N-dimethylformamide (DMF) was provided by Tedia. N,N-dimethylacetamide (DMA), dichloromethane (DCM), methanol (MeOH), 2,4,6-trinitrophenol (TNP), 2,4-dinitrophenol (2,4-DNP), p-nitrophenol (PNP), 2,4-dinitrotoluene (2,4-DNT), m-dinitrobenzen (m-DNB), nitrobenzene (NB) and 4-nitrotoluene (4-NT) were supplied by Sinopharm.

Characterization

The FTIR spectra were recorded from KBr pellets in the range 4000-400 cm^{-1} on Nicolet 5700 spectrometer. Powder X-ray diffraction (PXRD) data were collected from 3° to 50° with a step of 0.02° on XRD diffractometer (D8 Discover, Bruker-AXS) and Rigaku Smartlab with Cu-Kα radiation (λ = 1.54056 Å). The morphologies were collected through scanning electron microscopy (SEM, JSM-7800F). Transmission electron microscopy (TEM) images were taken by JEOL 2100Plus at 200 kV. Atomic force microscopy (AFM) images were taken using a Park XE-70. Thermogravimetric analyses (TGA) were carried out on a TA Instruments SDT-Q600 simultaneous DTA-TGA under N_2 at a heating rate of 10 °C/min. The photo-luminescence spectra were recorded on a HORIBA Fluoromax-4 fluorescence spectrometer. Dynamic light scattering (DLS) was measured on a 90 Plus particle size analyzer (Brookhaven Instruments, USA). The lifetime was measured using Edinburgh FLSP920 fluorescence spectrophotometer equipped with a nanosecond hydrogen flash-lamp (nF920) and a microsecond flash-lamp (μF900).

Synthesis of La-TCA Crystals

The mixture of $La(NO_3)_3 \cdot xH_2O$ (406 mg, 1.25 mmol) and TCA (94 mg, 0.25 mmol) in 10 mL DMA, 4 mL water and 5 mL hydrochloric acid solution (pH = 1) were sealed in a 40 mL vial, heated to 100 °C and keep 24 h. After the mixture cooled to room temperature, the resultant light yellow crystals obtained were

washed with DMA and dried at room temperature (yield: 70% based on TCA ligands). The La-TCA bulk crystals were activated in a vacuum oven at 120 °C for 12 h to remove the DMA solvents and sealed for further use.

Synthesis of La-TCA Nanosheets

In a typical experiment, the activated La-TCA bulk crystals (5 mg) were ground for 5 min and then immersed into methanol solution with another 1 h sonication. Then the colloidal suspension obtained was then centrifuged for three times (1000 rpm for 5 min) to remove the large particles, and subsequently the upper liquid was collected by centrifugation (10000 rpm for 5 min).

X-ray Crystallography of La-TCA

The crystallographic data collections for La-TCA were carried out on a Bruker Smart Apex II CCD area detector diffractometer with graphite-monochromated Mo Kα radiation (λ = 0.71073 Å) at 296(2) K using the ω-scan technique. The diffraction data were integrated using the SAINT program, which was also used for the intensity corrections for the Lorentz and polarization effects. A semi-empirical absorption correction was applied using the SADABS program. The structure of La-TCA was solved by direct method and all the non-hydrogen atoms were refined anisotropically on F^2 by the full-matrix least-squares technique using the SHELXL-2014 crystallographic software package. All the hydrogen atoms were generated geometrically and refined isotropically using the riding model. In the asymmetric unit of La-TCA, two coordinated DMA solvents were disordered and refined with the 'part' order. The details of the crystal parameters, data collection and refinements for La-TCA bulk crystals are summarized in Table S1.

Fluorescence Sensing Experiment

La-TCA nanosheets (10 mg) were immersed in different organic solvents (25 mL) followed by ultrasonication treatment for 5 min, and sampling 3 mL (~0.5 mM) stable emulsions for measurements. Then, different NACs in DMF solution were added into the La-TCA emulsion for the luminescence detection (TNP, 2,4-

DNP, and PNP with 2×10^{-3} mol/L; 2,4-DNT, 4-NT and m-DNB with 2×10^{-2} mol/L; NB with 2×10^{-1} mol/L) at room temperature. After sensing experiment, the La-TCA nanosheets were collected from the solutions by high-speed centrifugation (10000 rpm for 5 min). The recycled nanosheets were washed with methanol solution, and then collected by centrifuge at 10000 rpm for 5 min.

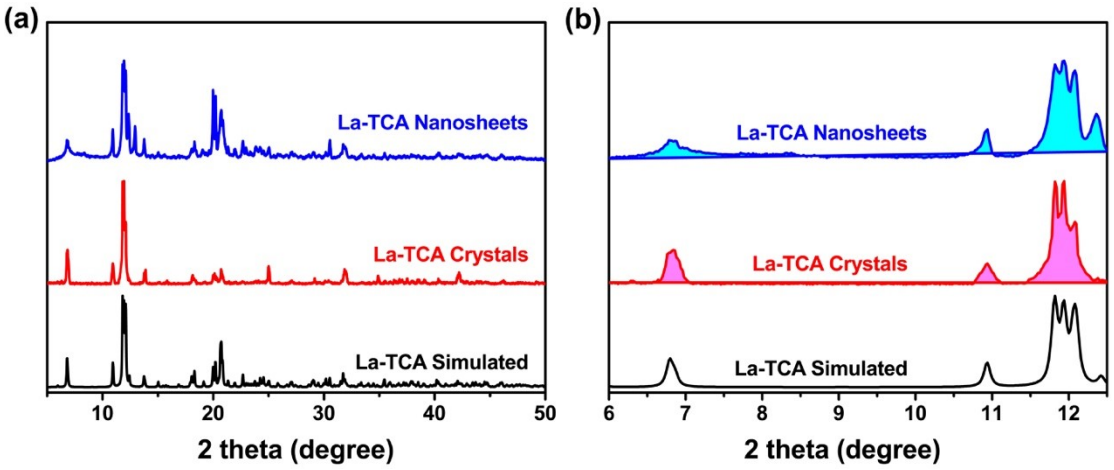

Fig. S1 (a) PXRD patterns of the simulated, La-TCA bulk crystals and La-TCA nanosheets. (b) Magnified PXRD patterns of the simulated, La-TCA bulk crystals and La-TCA nanosheets between 6° and 12.5°.

By magnifying the PXRD patterns of La-TCA between 6° and 12.5° (Fig. S1b), it can be found more clearly that La-TCA crystals show obvious diffraction peaks at 6.8° (full-width at half-maximum, FWHM = 0.190), 10.9° (FWHM = 0.158) and 12° (triple peaks, FWHM = 0.269). For La-TCA nanosheets, although the diffraction peaks appear at the same position on PXRD patterns, the corresponding FWHM changes to 0.344, 0.133 and 0.393 respectively, which indicates that the diffraction peaks are obviously broadened compared with La-TCA crystals.

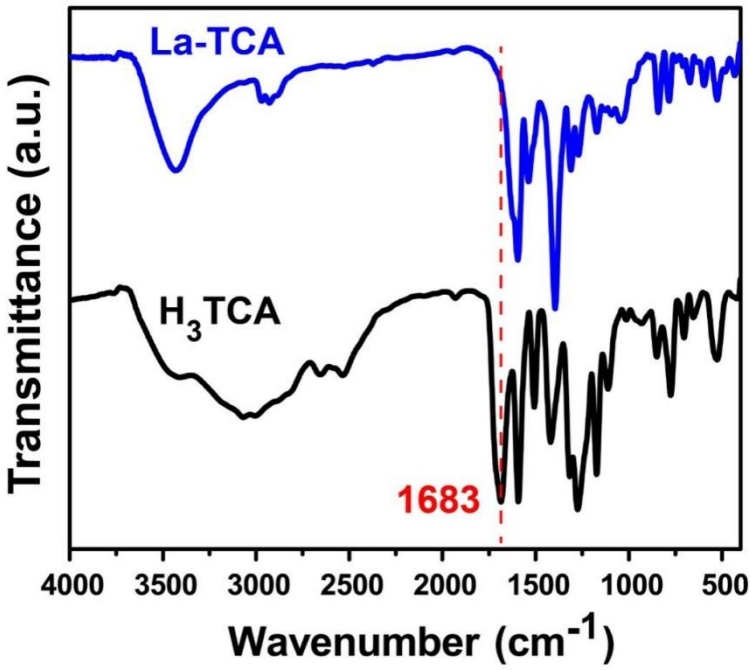

Fig. S2 FTIR spectra of TCA ligand and bulk La-TCA.

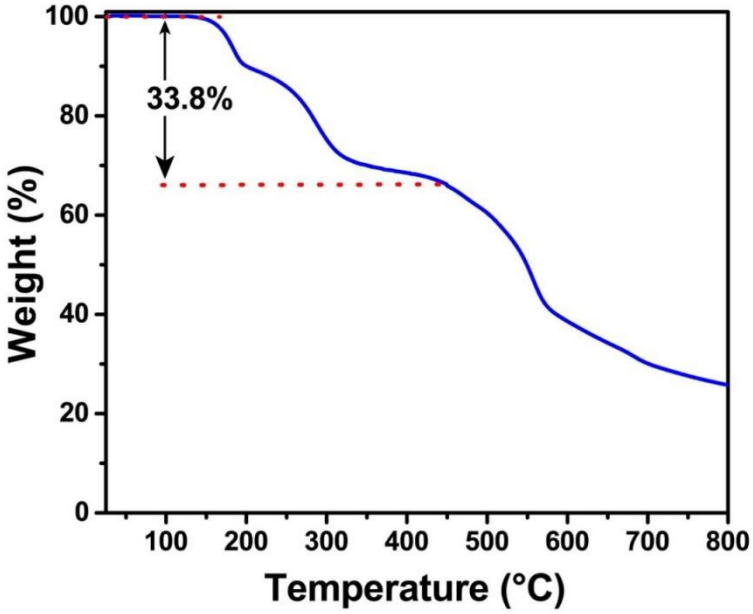

Fig. S3 TGA curve of bulk La-TCA from 30 ^{o}C to 800 ^{o}C.

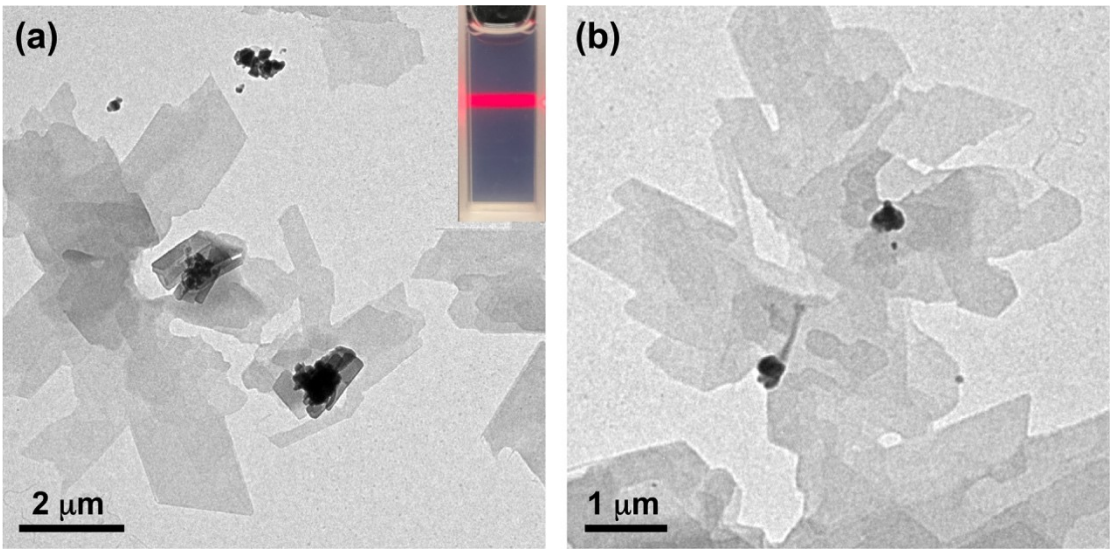

Fig. S4 (a) and (b) Low-magnification TEM images of La-TCA nanosheets. Inset in (a): Photograph of the Tyndall effect of La-TCA nanosheets in MeOH solution.

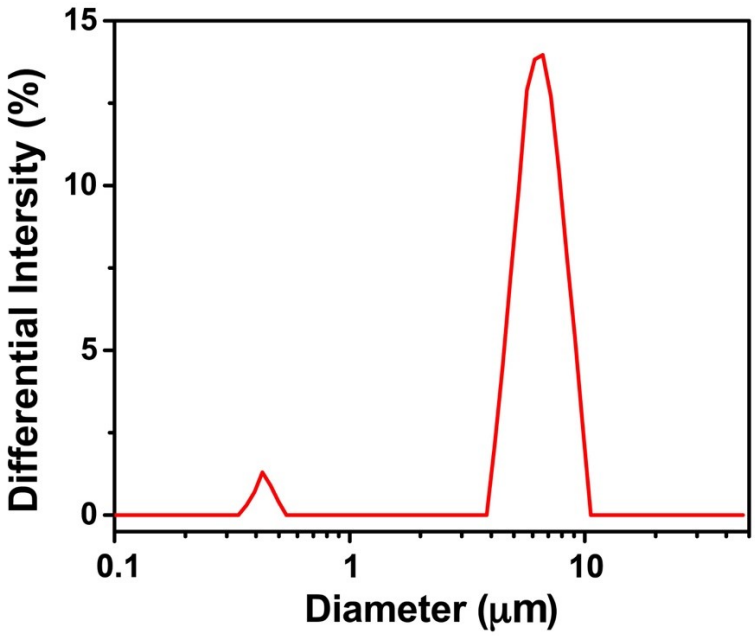

Fig. S5 The dynamic light scattering (DLS) experimental data on the colloidal solution of La-TCA nanosheets.

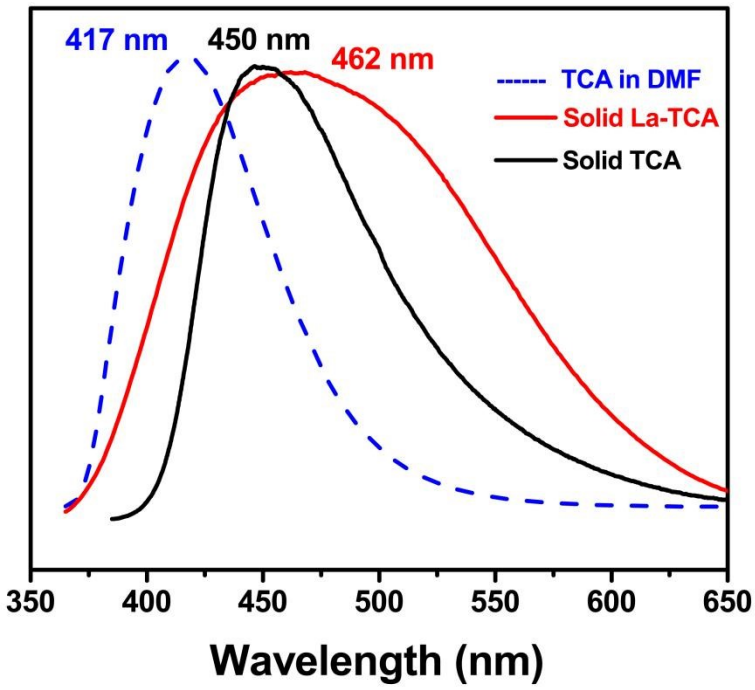

Fig. S6 Emission spectra of TCA ligand and La-TCA in solid state as well as TCA dispersed in DMF solvent (λ_{ex} 375 nm).

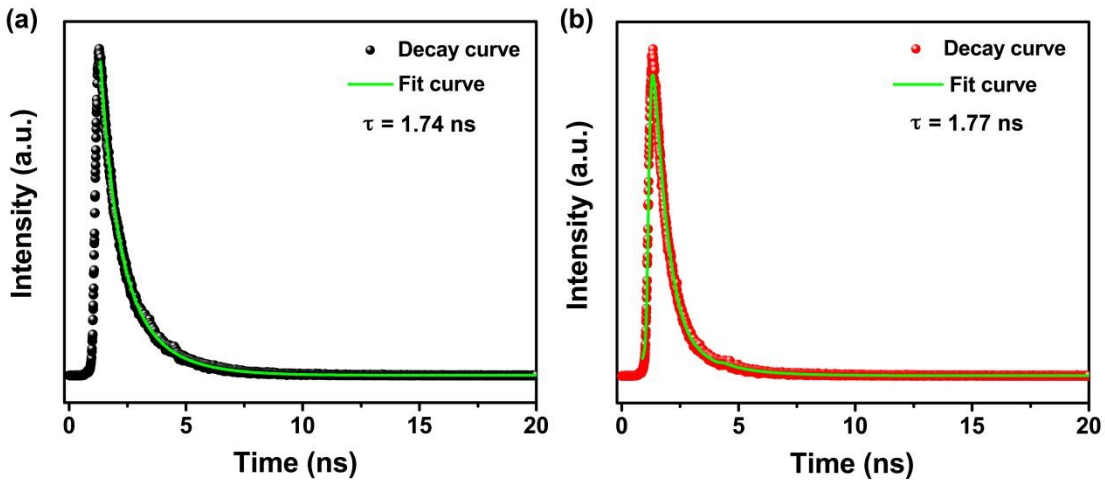

Fig. S7 Photoluminescence decay curves of (a) TCA ligands and (b) La-TCA nanosheets.

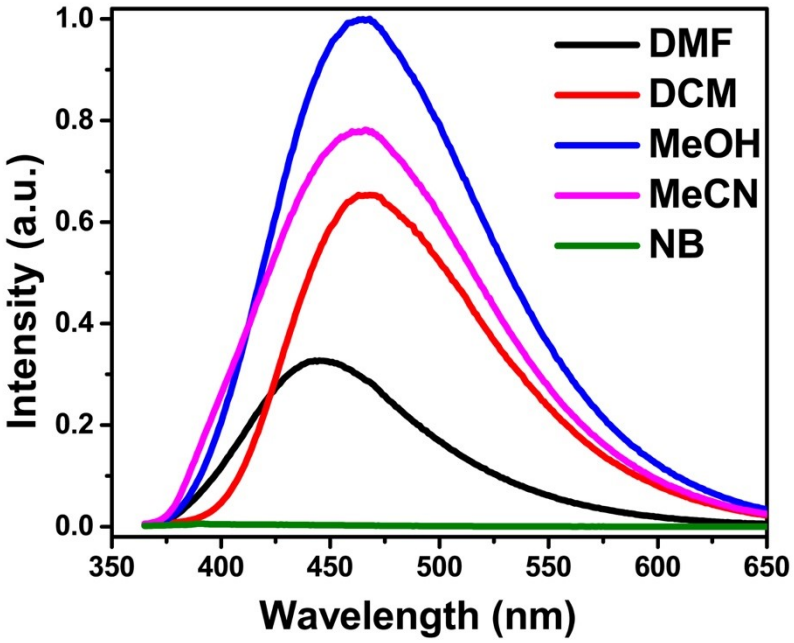

Fig. S8 Emission spectra of La-TCA in different solvents (λ_{ex} 375 nm).

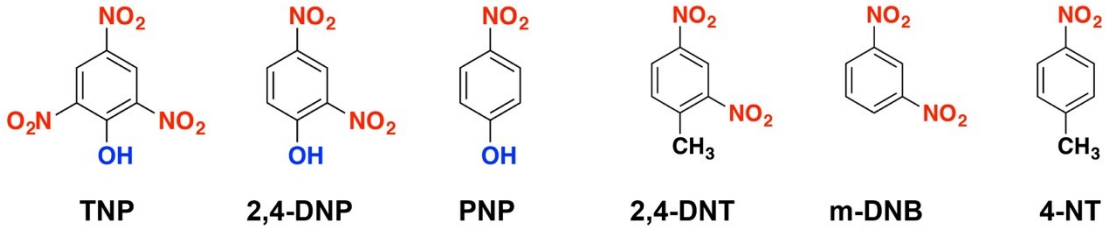

Fig. S9 Molecular structure information of various NACs.

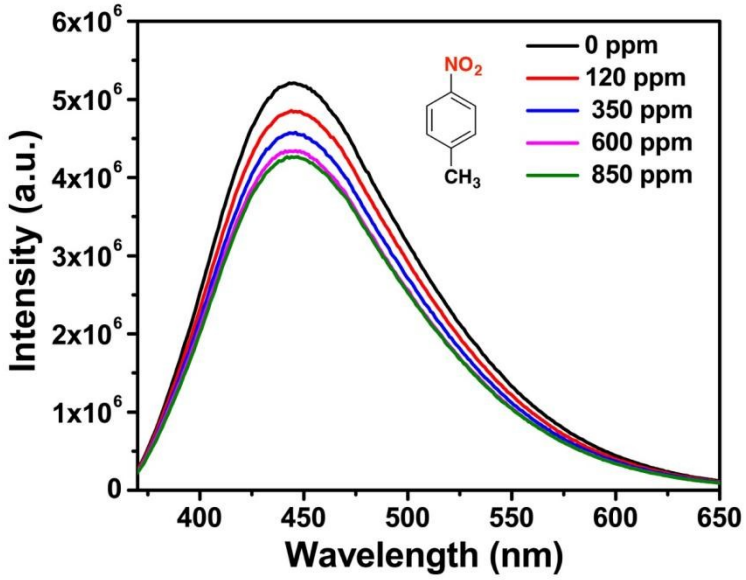

Fig. S10 Fluorescent spectra of La-TCA nanosheets suspended in DMF solvent with different concentrations of 4-NT.

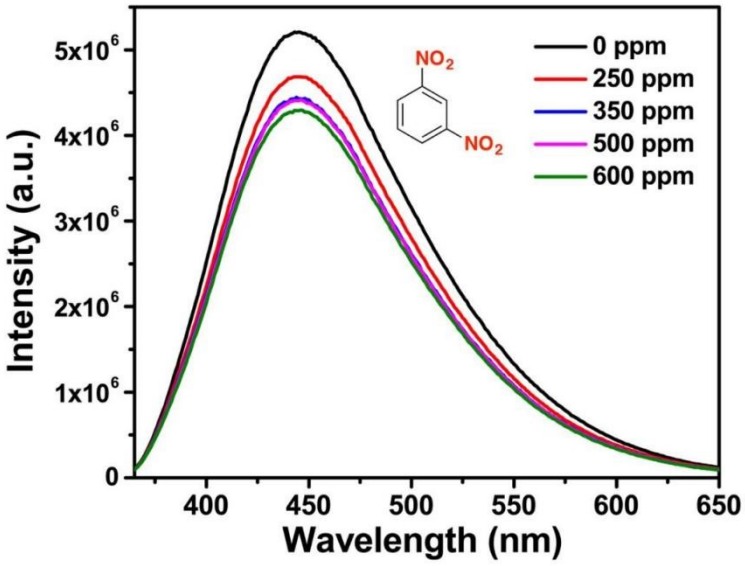

Fig. S11 Fluorescent spectra of La-TCA nanosheets suspended in DMF solvent with different concentrations of m-DNB.

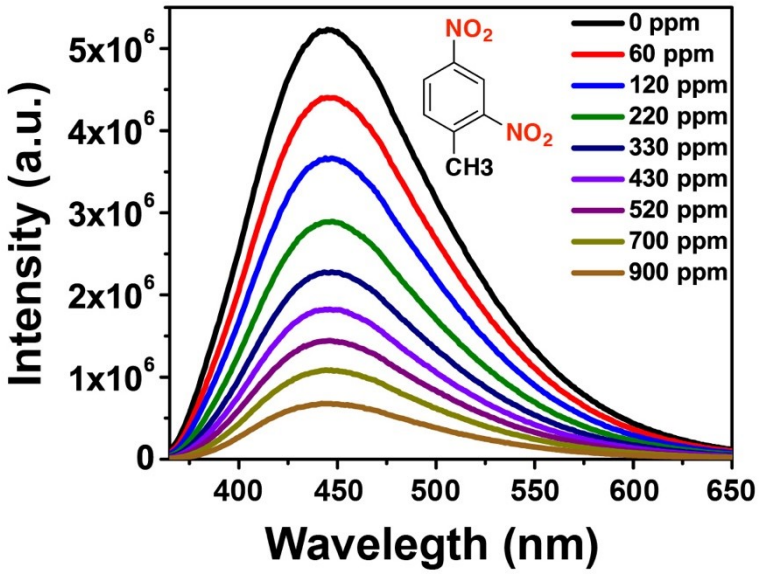

Fig. S12 Fluorescent spectra of La-TCA nanosheets suspended in DMF solvent with different concentrations of 2,4-DNT.

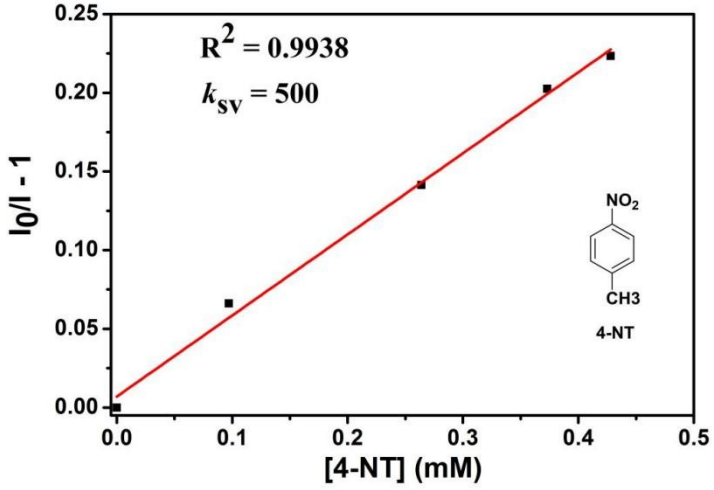

Fig. S13 SV plot of La-TCA nanosheets for 4-NT.

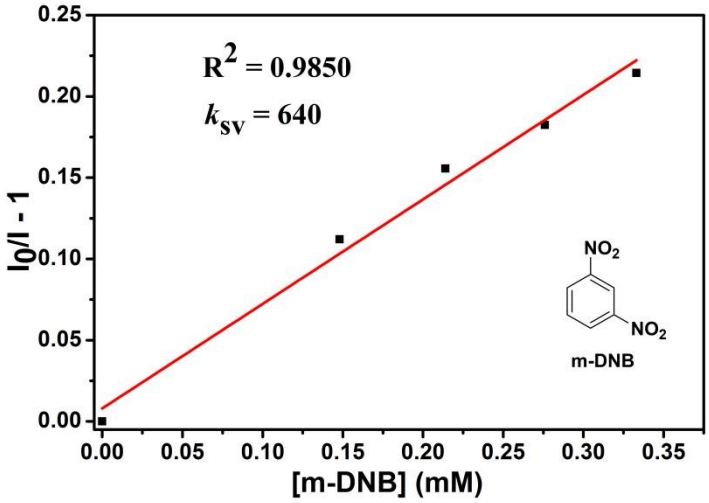

Fig. S14 SV plot of La-TCA nanosheets for m-DNB.

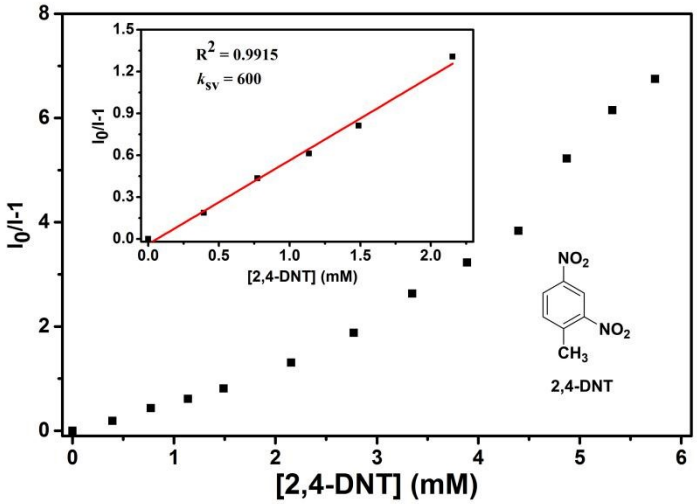

Fig. S15 SV plot of La-TCA nanosheets for 2,4-DNT.

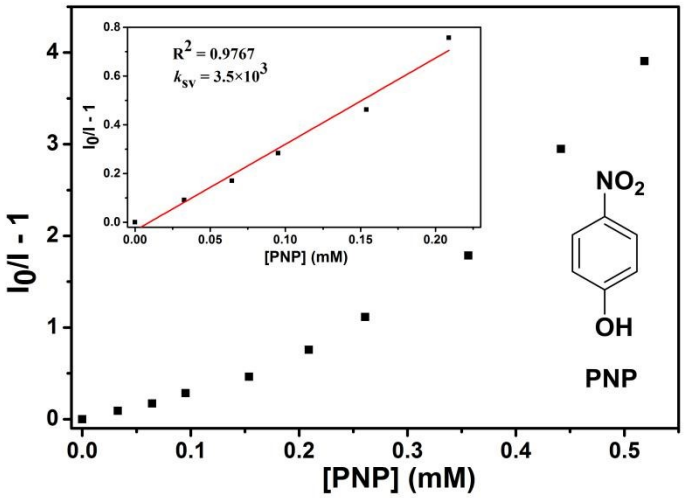

Fig. S16 SV plot of La-TCA nanosheets for PNP. Inset: in the low concentration region.

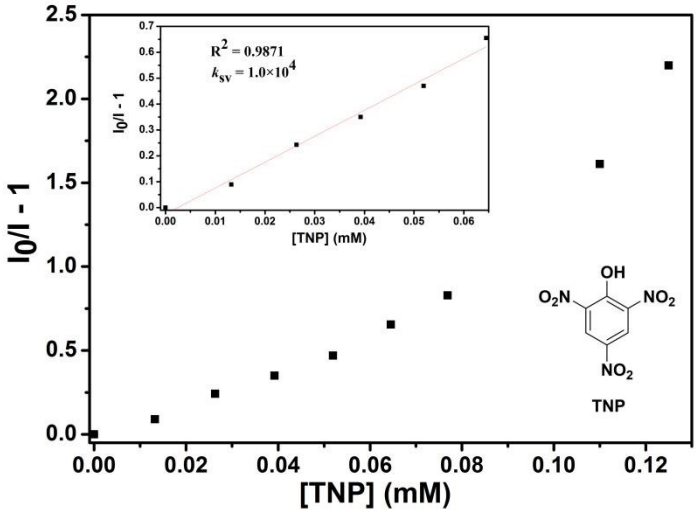

Fig. S17 SV plot of La-TCA nanosheets for TNP. Inset: in the low concentration region.

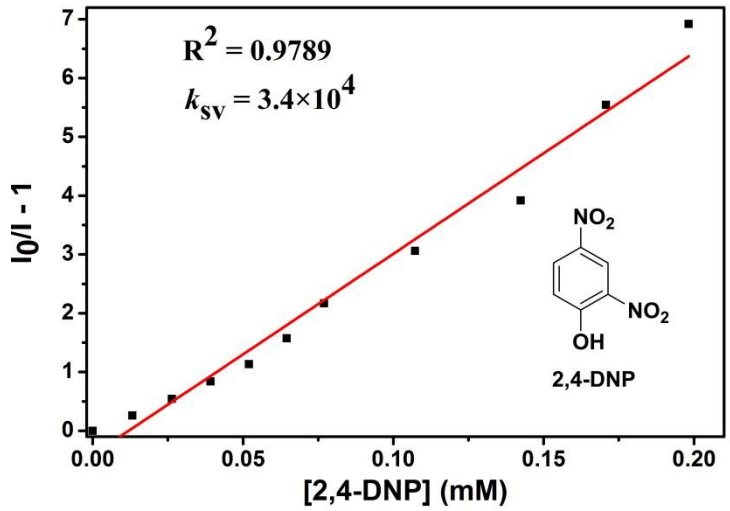

Fig. S18 SV plot of La-TCA nanosheets for 2,4-DNP.

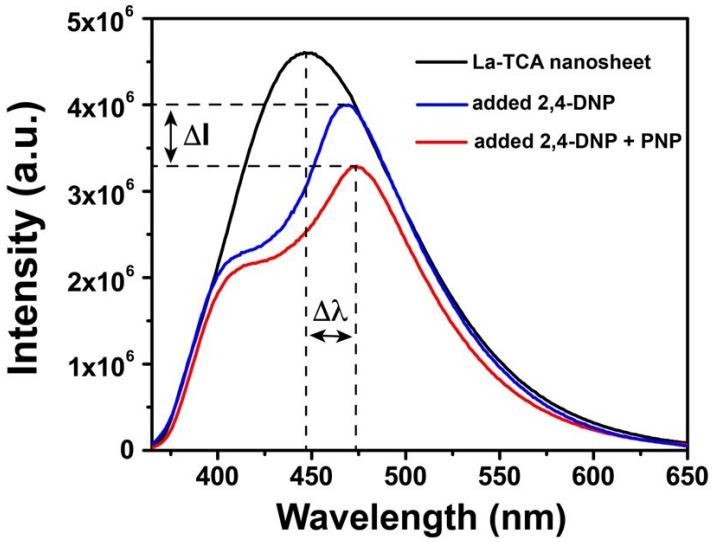

Fig. S19 Emission spectra of La-TCA nanosheets after adding 10 ppm 2,4-DNP and 10 ppm PNP.

La-TCA nanosheets can be used to distinguish 2,4-DNP and PNP from the hybrid mixture. 2,4-DNP can be identified by the wavelength shift ($\Delta\lambda$= 25 nm), and then PNP can be distinguished according to the changes of additional intensity (ΔI about 15%).

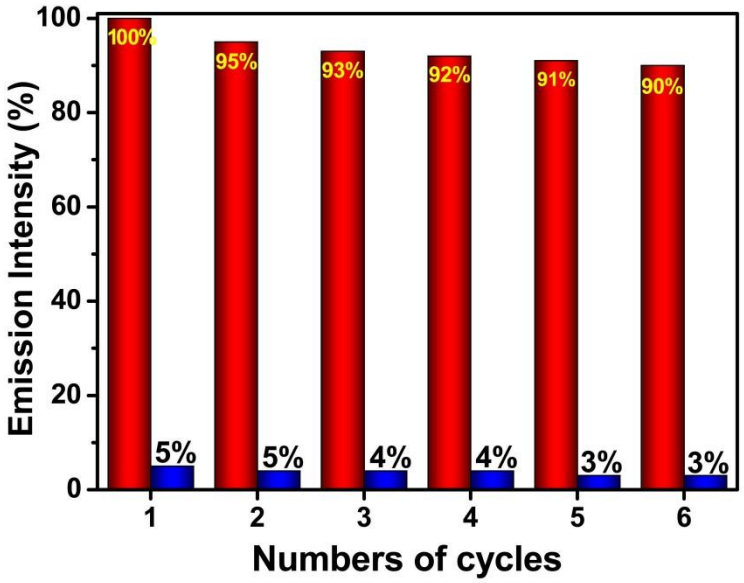

Fig. S20 The quenching and recyclability test of La-TCA nanosheets. The red bars represent the initial luminescence intensity and the blue bars represent the intensity upon addition of 2,4-DNP.

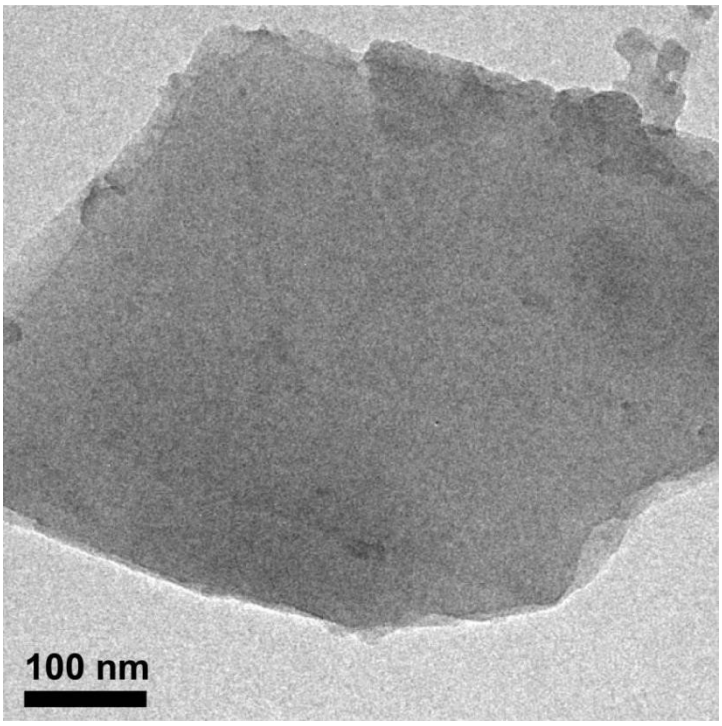

Fig. S21 TEM image of La-TCA nanosheets after recyclability test.

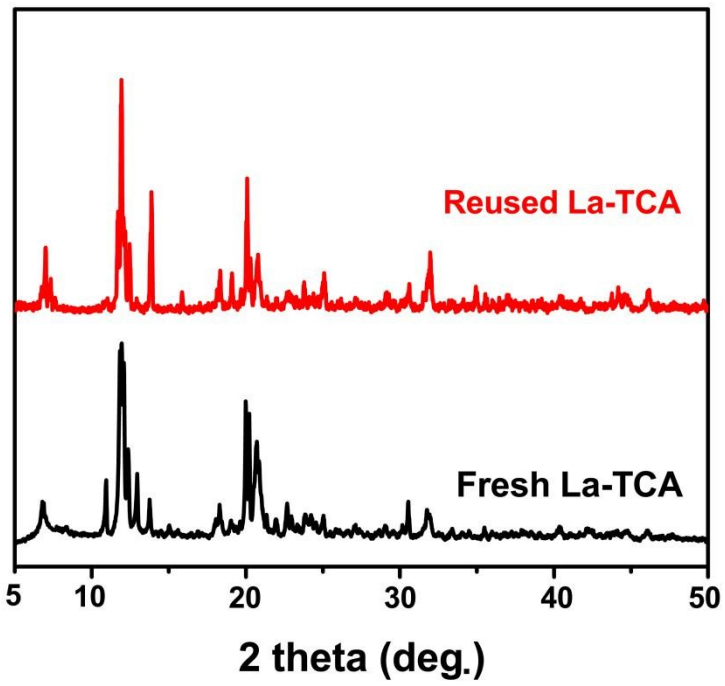

Fig. S22 PXRD patterns of La-TCA nanosheets after recyclability test.

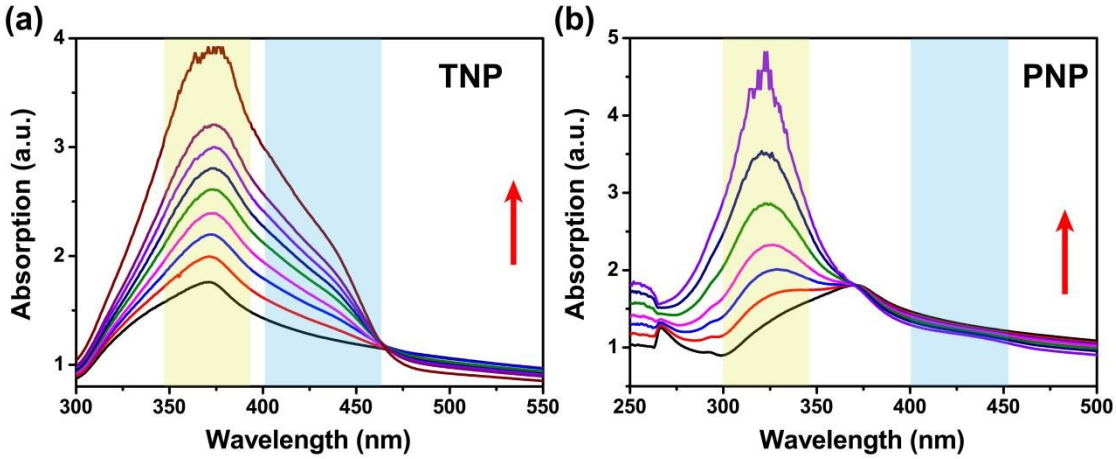

Fig. S23 In-situ UV-vis spectroscopy of La-TCA for (a) TNP and (b) PNP during the titration process.

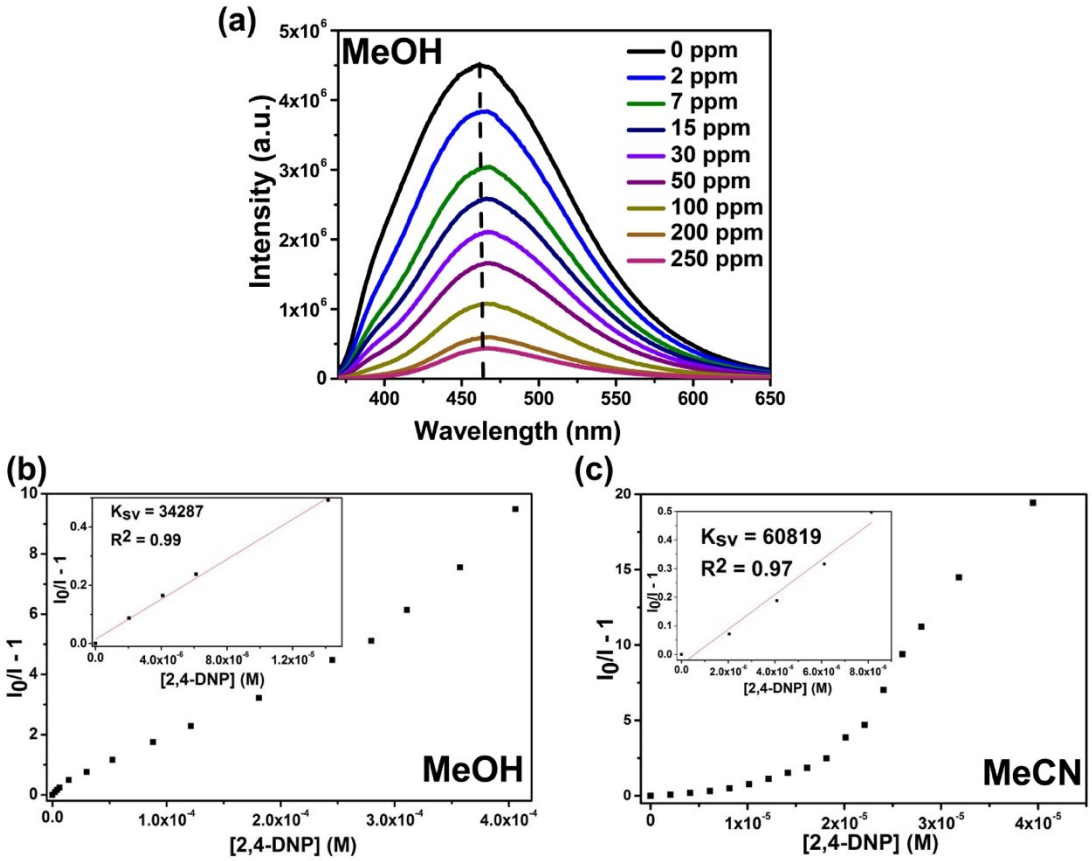

Fig. S24 (a) Fluorescence intensity of the La-TCA nanosheets in MeOH solution upon addition of 2,4-DNP. SV plots of La-TCA nanosheets for 2,4-DNP in (b) MeOH and (c) MeCN solution.

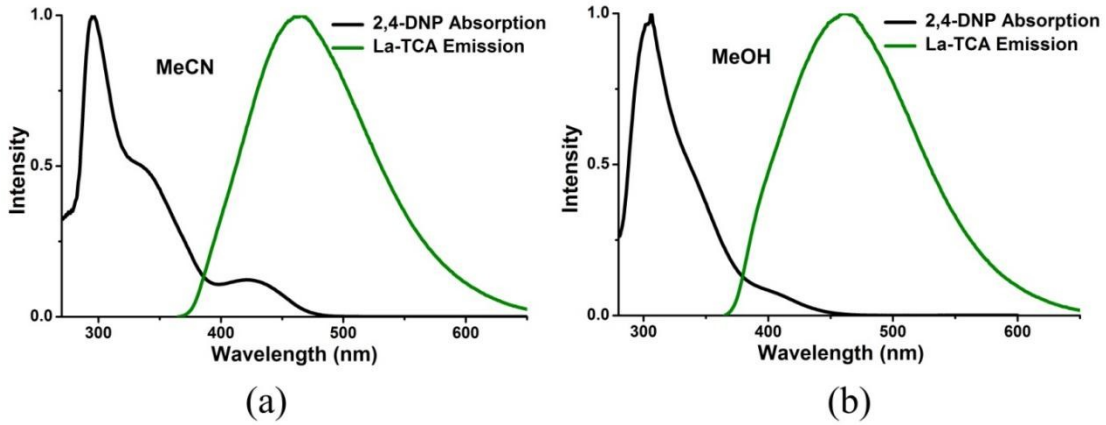

Fig. S25 Spectral overlap between 2,4-DNP absorption spectrum and La-TCA nanosheets emission spectrum in (a) MeCN and (b) MeOH.

Table S1. Crystal data and structure refinements of La-TCA.

Compound	**La-TCA**
Empirical formula	$C_{33}H_{39}LaN_4O_9$
Formula weight	774.59
Temperature/K	296(2)
Crystal system	Orthorhombic
Space group	*pbca*
a/Å	26.011(5)
b/Å	8.8798(16)
c/Å	29.636(5)
α/°	90
β/°	90
γ/°	90
V/Å^3	6845(2)
Z	8
Dc/(g cm^{-3})	1.503
F(000)	3152
θ range for data collection/°o	1.58-28.27
Reflections collected	46524
Unique reflections	5974
Goof	1.062
R_1[a] [I > 2σ(I)]	0.0461
wR_2[b] [I > 2σ(I)]	0.029

[a] $R_1 = \Sigma||F_o|-|F_c||/\Sigma|F_o|$.

[b] $wR_2 = |\Sigma w(|F_o|^2-|F_c|^2)|/\Sigma|w(F_o)^2|^{1/2}$, where $w = 1/[\sigma_2(F_o^2) + (aP)^2 + bP]$. $P = (F_o^2 + 2F_c^2)/3$.

Table S2. Comparison of CP/MOF sensors for detecting NACs.

CPs/MOFs	Analytes	*K*sv (M^{-1})	LODs	References
	2,4-DNP	**34000**	**0.55 ppm**	**this work**
La-TCA	**TNP**	**10000**	**1.9 ppm**	**this work**
	PNP	**3500**	**1.9 ppm**	**this work**
Cd-NTB	TNP	200000	/	2
Sc-EBTC	2,4-DNP	28500	5.71 ppb	3
	PNP	27500	6.26 ppb	
Zn-MTAIA	PNP	10300	/	4
Zr-NDI	TNP	40570	8.1 ppm	5
BUT-12	TNP	21000	23 ppb	6
Cd-MOF	2,4-DNP	23700	0.84 ppm	7
	TNP	16100	1.57 ppm	
Eu-MOF	2,4-DNP	6160	16.4 μmol L^{-1}	8
Tb-MOF	2,4-DNP	7750	16.2 μmol L^{-1}	
FCS-2	PNP	820	/	9
	2,4-DNP	14300	/	
	TNP	38200	/	

References

1. P. Wu, Y. Li, J.-J. Zheng, N. Hosono, K. Otake, J. Wang, Y. Liu, L. Xia, M. Jiang, S. Sakaki, S. Kitagawa. Carbon dioxide capture and efficient fixation in a dynamic porous coordination polymer. *Nat. Commun.*, **2019**, *10*, 4362.

2. Z.-Q. Shi, N.-N. Ji, H.-L. Hu. Luminescent triphenylamine-based metal–organic frameworks: recent advances in nitroaromatics detection. *Dalton Trans.*, **2020**, *49*, 12929–12939.

3. D. Zhan, A. Saeed, Z. Li, C. Wang, Z. Yu, J. Wang, N. Zhao, W. Xu, J. Liu. Highly fluorescent scandium-tetracarboxylate frameworks: selective detection of nitro-aromatic compounds, sensing mechanism, and their application. *Dalton Trans.*, **2020**, *49*, 17737–17744.

4. P. Dasa, S. K. Mandal. A highly emissive fluorescent Zn-MOF: molecular decoding strategies for solvents and trace detection of dunnite in water. *J. Mater. Chem. A*, **2018**, *6*, 21274–21279.

5. G. Radha, T. Leelasree, D. Muthukumar, Renjith S. Pillai, H. Aggarwal. Highly selective detection of TNP over other nitro compounds in water: the role of selective host–guest interactions in Zr-NDI MOF. *New J. Chem.*, **2021**, *45*, 12931–12937.

6. B. Wang, X.-L. Lv, D. Feng, L.-H. Xie, J. Zhang, M. Li, Y. Xie, J.-R. Li, H.-C. Zhou. Highly stable zr(iv)-based metal–organic frameworks for the detection and removal of antibiotics and organic explosives in water. *J. Am. Chem. Soc.,* **2016**, *138*, 6204–6216.

7. L. Lu, J. Wu, J. Wang, J.-Q. Liu, B.-H. Li, A. Singh, A. Kumar, S. R. Batten. An uncommon 3D 3,3,4,8-c Cd(II) metal–organic framework for highly efficient luminescent sensing and organic dye adsorption: experimental and theoretical insight. *CrystEngComm*, **2017**, *19*, 7057–7067.

8. Z.Sun, Y. Li, Y. Ma, L. Li. Dual-functional recyclable luminescent sensors based on 2D lanthanide-based metal-organic frameworks for highly sensitive detection of Fe^{3+} and 2,4-dinitrophenol. *Dyes Pigm.*, **2017**, *146*, 263–271.

9. M.-M. Chen, X. Zhou, H.-X. L, X.-X. Yang, J.-P. Lang. Luminescent two-dimensional coordination polymer for selective and recyclable sensing of nitroaromatic compounds with high sensitivity in water. *Cryst. Growth Des.,* **2015**, *15*, 2753–2760.